Weather and Climate Extremes 37 (2022) 100483

Contents lists available at ScienceDirect

Weather and Climate Extremes

journal homepage: www.elsevier.com/locate/wace

Tropical cyclone climatology, variability, and trends in the Tonga region, Southwest Pacific

Moleni Tu'uholoaki [a,d,*], Awnesh Singh [a], Antonio Espejo [b], Savin Chand [c], Herve Damlamian [b]

[a] Pacific Centre for Environment and Sustainable Development, The University of the South Pacific, Suva, Fiji
[b] Geoscience, Energy and Maritime Division, Pacific Community, Fiji
[c] Institute of Innovation, Science and Sustainability, Federation University, Mt Helen Campus, Victoria, Australia
[d] Tonga Meteorological Service, Tonga

ARTICLE INFO

Keywords:
Tropical cyclones
Tonga
Variability
Climatology
Trends
ENSO

ABSTRACT

The focus of several past tropical cyclone (TC) studies in the Southwest Pacific (SWP) had been primarily at the regional scale, with little or no attention to the local-scale TC activity (i.e., at the country level). With the growing coastal population in the South Pacific Island countries, as well as increasing threats from and exposure to climate extremes mostly affecting vulnerable communities, examining TC-related risks at the country level is more imperative now than before. This study catalogues for the first time the climatology, variability and trends of TCs affecting Nuku'alofa, the capital of Tonga using the Southwest Pacific Enhanced Archived for Tropical Cyclone (SPEArTC) dataset for the period between 1970 and 2019. The variability is examined in relation to the El Niño–Southern Oscillation (ENSO) phenomenon, which is the major driver of the year-to-year variability of TC activity in the SWP. A total of 128 TC tracks affected the Tonga region over the study period, with a seasonal average of ~2.6 TCs per year. Of these, about 50% occurred during the peak months of January and February, and ~38.8% of the total were of hurricane intensity (Categories 3, 4 and 5). Although differences were found between the average number of TCs per year during El Niño, La Niña and ENSO-neutral events (~2.9, ~2.6 and ~2.3, respectively), they were statistically insignificant. No significant long-term trends were found in the number of TCs, severe TCs, and accumulated cyclone energy (ACE) over the period of study. The findings of this study will provide the information needed for disaster preparedness and TC predictions in Tonga.

CRediT author statement

Moleni Tu'uholoaki: Conceptualization, Methodology, Software, Visualisation, writing-original, reviewing and editing. Awnesh Singh: Supervision, Conceptualization, Methodology, Visualisation, Validation, writing-reviewing and editing. Antonio Espejo: Supervision, Methodology, Conceptualization, Visualisation, software, validation and editing. Savin Chand: Supervision, software, writing-reviewing and editing. Herve Damlamian: Supervision, resources, validation and editing.

1. Introduction

Tropical Cyclones (TCs) frequently affect the livelihoods of people in the South Pacific Island countries (Terry, 2007). Associated conditions such as torrential rain, strong winds and storm surges are mostly responsible for damages caused during a TC event. As a result, a country's economic and social development are consistently hindered and can often cost millions of dollars each year to recover and mitigate the impacts of TCs (Terry, 2007; Lavender and Dowdy, 2016; Magee et al., 2016). Moreover, with the alarming rate of sea-level rise in the Pacific (Nurse et al., 2014; Nerem et al., 2018), coupled with the projections of more severe TCs in the future (Christensen et al., 2013; Walsh et al., 2016; Knutson et al., 2020), the poleward migration of TCs (Kossin et al., 2014; Daloz and Camargo, 2018; Sharmila and Walsh, 2018; Knutson et al., 2020) and the global slowdown of TC translation speed (Kossin, 2018, 2019; Lanzante, 2019; Moon et al., 2019; Zhang et al., 2020; Emanuel, 2021) due to human-induced global warming, TC risks are likely to exacerbate further for the small island nations in the South Pacific, such as Tonga. For instance, Tonga recently has been affected by two major severe TCs - TC Ian on January 11, 2014, which incurred damage equivalent to 11% of Tonga's Gross Domestic Product (GDP)

* Corresponding author. Pacific Centre for Environment and Sustainable Development, The University of the South Pacific, Suva, Fiji.
E-mail address: molenit@gmail.com (M. Tu'uholoaki).

https://doi.org/10.1016/j.wace.2022.100483
Received 4 January 2022; Received in revised form 6 July 2022; Accepted 7 July 2022
Available online 12 July 2022

and TC Gita on February 12, 2018, which inflicted damage around 38% of Tonga's GDP (World Trade Organisation, 2018). However, due to the lack of country-specific information on TC activity, objective assessment of such risks is difficult and often challenging. Our emphasis here, therefore, is to bridge the gap by providing a comprehensive understanding of TC characteristics in the Tonga region.

In the Southwest Pacific (SWP), the South Pacific Convergence Zone (SPCZ), which is obliquely oriented along the northwest-southeast axis in the southwest tropical Pacific (Singh et al., 2011), is often considered an incubation zone of TCs (Vincent et al., 2011; Jourdain et al., 2011; Menkes et al., 2012; Diamond et al., 2013; Brown et al., 2020) as the areas within 10° poleward of the mean SPCZ position have conditions that are favourable for TC genesis (Gray, 1975; Basher and Zheng, 1995; Kuleshov et al., 2008; Ramsay et al., 2008; Vincent et al., 2011; Widlansky et al., 2019; Brown et al., 2020). The SPCZ is very active during November–April (Kuleshov et al., 2009; Vincent et al., 2011; Hartfield et al., 2018; Blunden and Arndt, 2019), which coincides with the Southern Hemisphere TC season.

The El Niño-Southern Oscillation (ENSO) phenomenon is a leading mode of interannual climate variability in the tropical Pacific (Zheng, 2019) and is known to influence TC activity in the SWP (Basher and Zheng, 1995; Chand and Walsh, 2009; Kuleshov et al., 2009; Vincent et al., 2011; Dowdy et al., 2012; Ramsay et al., 2012; Magee et al., 2017; Kuleshov et al., 2020), and the movement of the SPCZ (Folland et al., 2002; Vincent et al., 2011). During El Niño (the warm phase of ENSO), the SPCZ shifts northeastward and becomes more zonally oriented relative to its climatological location, while during La Niña (the cold phase of ENSO), the SPCZ shifts southwestward of its climatological location (Folland et al., 2002; Vincent et al., 2011; Haffke and Magnusdottir, 2013; Salinger et al., 2014; Magee et al., 2017; Wang et al., 2017). These ENSO-related shifts in the SPCZ position subsequently affect TC genesis locations (Hastings, 1990; Chu, 2004; Terry, 2007; Kuleshov et al., 2008, 2009; Terry and Gienko, 2010; Vincent et al., 2011; Dowdy et al., 2012; Iizuka and Matsuura, 2012; Chand et al., 2013; Diamond et al., 2013, 2015; Brown et al., 2020; Sharma et al., 2020), causing variations in TC activity between different island countries in the Pacific such as Fiji, Samoa and Tonga (the FST region).

Most countries that lie in the vicinity of the mean position of the SPCZ often experience enhanced TC activity during the El Niño years compared to La Niña years (Chand and Walsh, 2009, 2010; Kuleshov et al., 2009; Dowdy et al., 2012; Iizuka and Matsuura, 2012; Chand et al., 2013; Kuleshov et al., 2020). In addition, countries that lie further south of the mean SPCZ location, often experience enhanced TC activity during La Niña years compared to El Niño years. However, the Tonga region seems to be located in a neutral zone (e.g., Basher and Zheng, 1995). Hence in this study, we further investigate to what extent ENSO influences TC activity in the Tonga region. It is worth noting that there are also other modes of climate variabilities that influence TC activities in the SWP (e.g., Interdecadal Pacific Oscillation (IPO; Magee et al., 2017), Southern Annular Mode (SAM; Diamond and Renwick, 2015) and Indian Ocean sea surface temperature (SST) variability (Magee and Verdon-Kidd, 2018).

Several efforts have been made over the past decades to improve our understanding of the impact of anthropogenic-induced climate change on TC trends at global and hemispheric scales (e.g., Webster et al., 2005; Kuleshov et al., 2009; 2010; Knutson et al., 2019; Moon et al., 2019), regional scale (e.g., Kuleshov et al., 2009, 2010; Terry and Gienko, 2010; Knutson et al., 2019; Moon et al., 2019) and sub-regional scale (e.g., Basher and Zheng, 1995; Maru et al., 2018; Tauvale and Tsuboki, 2019). However, the lack of long-term homogeneous TC data and the presence of large natural variability often make detection and attribution of TC trends challenging in the Pacific, particularly at a subregional scale. Based on recent data, the overall trend in the number of total TCs, as well as the number of severe TCs (i.e., those greater than Category 3; 10-min averaged winds >63 knots) in the SWP are very weak and statistically insignificant (Kuleshov et al., 2010; Ramsay, 2017; Chand et al., 2020).

We note that the focus of most of the earlier studies was primarily on the characteristics of TCs spanning the greater SWP region, with little emphasis on quantifying the level of risks TCs pose at a country scale. Those that did focus on the island-scale TC risks (e.g., Kuleshov et al., 2020; Magee et al., 2020) were often constrained to the development of early warning forecast systems with ENSO as the main predictor. Using an additional and updated dataset for the period 1970 to 2019, this study aims to characterize TCs affecting the Tonga region, with the main emphasis on TC climatology, natural variability and trends. The objective is to provide information that would help the Tonga Meteorological Service to better understand the characteristics of TCs affecting Tonga and how ENSO affects these characteristics and hence improve the seasonal tropical cyclone forecasting and support their early warning forecasting system. In addition, local planners, insurers, teachers, researchers, disaster managers, builders, and engineers may benefit too from this climatological information. Furthermore, the study may help to bridge the gap in the literature for TCs between small island developing states in the South Pacific with those in other TC basins.

2. Data and methodology

2.1. TC track data

We define the Tonga region as the area covered by a 5° (or about 500 km) radius centred on Nuku'alofa, the capital of Tonga. Any TC track crossing this circle is considered to have affected the Tonga region. The size of the Tonga region is chosen in a way to contain all TC tracks with potential impacts including extreme waves on Tongatapu, the main island of Tonga, noting the diameter of TCs ranges from 200 to 1 000 km (WMO, 2022). Fig. 1 illustrates 128 tracks affecting the Tonga region, showing where they originated from, where they entered and exited the Tonga region and where they terminated to provide an overview of how dynamic and active TCs in this region are.

Tonga is located in the SWP, an archipelago comprising 169 islands of which 36 are inhabited. There are roughly two parallel chains of islands in Tonga. The western chain of islands is mostly volcanic islands, while the eastern chain of islands is mostly coral islands. These archipelagic islands extend ~800 km latitudinally. The total surface land area is about 750 km^2, with Tongatapu being 260.5 km^2. The total population of Tonga is 100,209 (Tonga Government Statistics Department report, 2021), with nearly three-quarters residing in Tongatapu. Fiji lies to the northwest, Samoa to the north, Niue to the northeast and Kermadec Islands (New Zealand) to the southwest of Tongatapu. Tonga's GDP is about 0.5 billion USD and heavily relies on remittances and international donor partners, with agriculture and tourism, are the two main income commodities (World Bank, 2022).

In this study, we use the SWP TC classification scheme (Table 1, e.g., Sinclair, 2002; Chand and Walsh, 2009; WMO, 2021) to classify TCs into four categories: tropical depressions (TDs), gale, storm and hurricanes. We also merge the SWP TC classification scheme with the Australian TC category classification system as shown in Table 1.

The study considers historical TCs from 1969/70 to 2018/2019 seasons based on data quality analysis from the Southwest Pacific Enhanced Archive for Tropical cyclones (SPEArTC; Diamond et al., 2012) hosted at the Asia-Pacific Data-Research of the International Pacific Research Center at the University of Hawaii. Since TCs in the Southern Hemisphere are spread over the two calendar years (November–April), a TC season is defined from July of the first year to June of the second year, with the second year used to refer to a particular season. TCs in the Tonga region are those that either form or track within the 500 km radius of Nuku'alofa. TC genesis (decay) is defined as the first (last) track point in the SPEArTC dataset.

The SPEArTC dataset contains generally 6-hourly track information, increasing to a higher temporal resolution at 3-hourly intervals when the TC is close to landfall or near an island. It also comprises maximum 10-

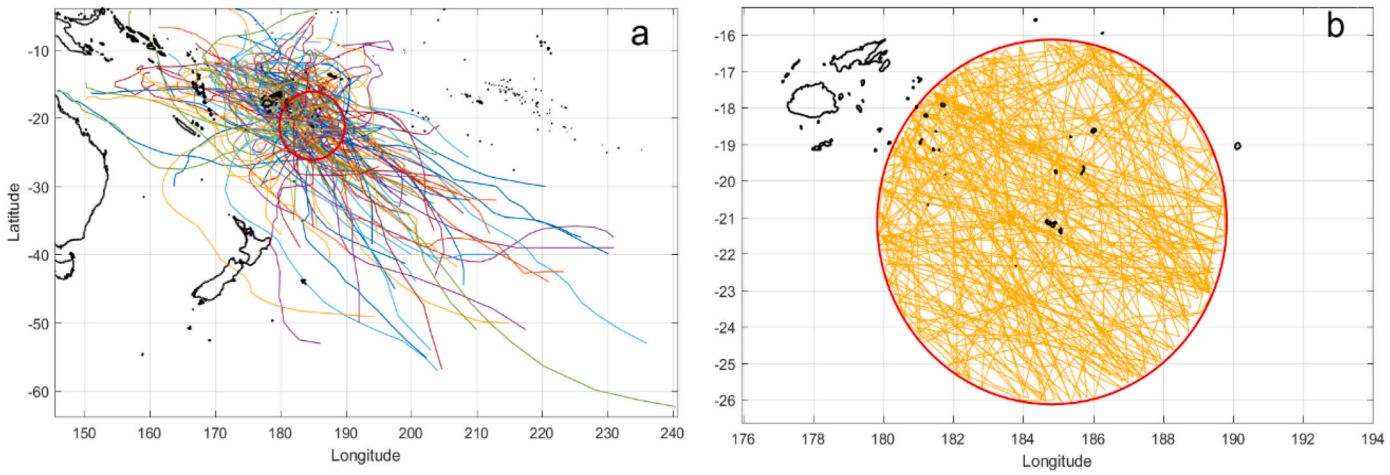

Fig. 1. a) A 5° radius circle (in red) centred on Nuku'alofa, Tonga, referred to as the Tonga region. All of the 128 TC tracks affecting the Tonga region between 1970 and 2019 are shown as coloured line plots. b) A close-up view of the Tonga region with TC tracks inside as orange line plots. (For interpretation of the references to colour in this figure legend, the reader is referred to the Web version of this article.)

Table 1
Classification of the SWP TCs combined with the Australian TC category classification system with 10-minuted averaged wind speed.

Classification of weather disturbances/Australian TC category classification system	Speed range (knots)
Tropical depressions	< 34
Tropical cyclones (Gale)/Category 1	34–47
Tropical cyclones (Storm)/Category 2	48–63
Severe Tropical cyclones (Hurricane)/Category 3	64–85
Severe Tropical cyclones (Hurricane)/Category 4	86–107
Severe Tropical cyclones (Hurricane)/Category 5	> 107

min averaged winds (in knots) and central pressures (in hPa) of available TC tracks in the SWP from 1840 to 2019 (see Fig. 2 for relationships between the variables), noting that the complete and reliable TC record for the SWP is available for the post-satellite era (i.e., ~1970 onwards; Holland, 1981; Diamond et al., 2012, 2013). Although satellite data was available since the late 1960s, it was first available for use in monitoring TCs in the South Pacific in 1969 (Terry and Gienko, 2010). All TC tracks were linearly interpolated to hourly data to maximise temporal representations of TC positions, maximum winds and pressures within the Tonga region, and to ensure no track is missed out.

For verification, named TCs affecting the Tonga region from the SPEArTC dataset were compared with a secondary data source from the Southern Hemisphere TC Data Portal (http://www.bom.gov.au/cyclone/tropical-cyclone-knowledge-centre/history/tracks/; see Fig. A1 in the Appendix). Both datasets had the same number of named TCs except for the years 1975, 2000, and 2016, simply due to SPEArTC continuing to provide track information even after the named TCs are downgraded to TDs, while the secondary data source ceases tracking at the last positions before they become TDs.

A total of 128 TCs (or ~20% of total TCs in the SWP) crossed the Tonga region over the study period and are included when analysing the spatial distributions of TCs. However, seven tracks were found to contain neither pressure nor wind information and were excluded from all analyses that involved TC intensities. Nine tracks had wind information but no corresponding pressure values, and so the missing pressure values were obtained empirically using the wind-pressure relationship in Fig. 2a. The best fit line (Fig. 2a) is a polynomial function of degree 2 with $R^2 = 0.9504$ and significant at the 95% confidence level. Its algebraic representation is given by Equation (1):

$$P = -0.002899V_m^2 + 0.4808V_m + 1014 \quad (1)$$

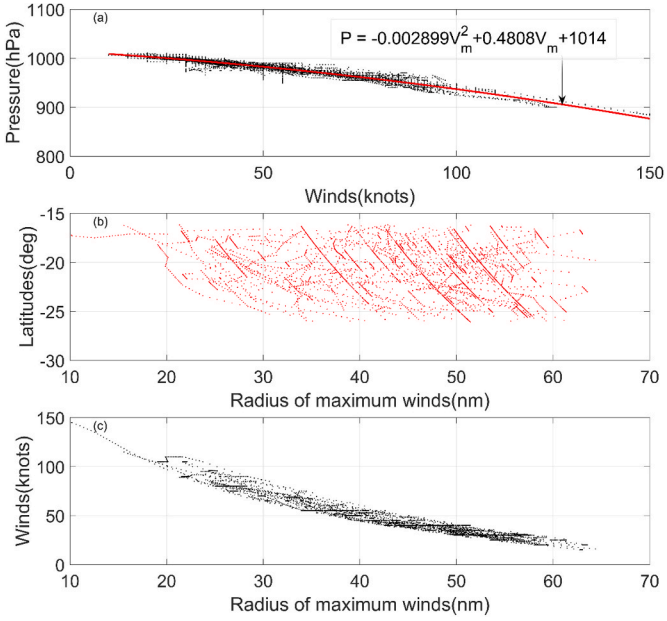

Fig. 2. (a) Wind vs pressure relationship from the SPEArTC database interpolated from 6-hourly to hourly for TCs in the Tonga region from 1970 to 2019. The red line is the best fit line for the data with the corresponding algebraic equation. (b) Relationship between radius of maximum winds with latitude. (c) Relationship between radius of maximum winds with intensity within the Tonga region. The unit for pressure is hPa, latitude is degrees, wind speed is knots, and the radius of maximum winds is nautical miles (nm). (For interpretation of the references to colour in this figure legend, the reader is referred to the Web version of this article.)

where P is the pressure in hPa and V_m is the maximum wind speed in knots.

Characteristics of TCs such as translational speeds and directions were derived using the hourly-interpolated positions of TCs. The Haversine formula for determining the distance between two track points, 1 h apart, was used to calculate the translational speed. The radius of maximum winds (RMW) is not available in the SPEArTC dataset so Equation (2) by Knaff et al. (2016) is used:

$$RMW = 218.3784 - 1.2014V_m + (V_m/10.9844)^2 - (V_m/35.3052)^3 - 145.5090\cos(\gamma) \quad (2)$$

where RMW is the radius of maximum winds in nautical miles, V_m is the maximum wind speed in knots, and γ is the latitude in degrees.

Fig. 2b&c illustrate the relationships between the radius of maximum winds with latitude and intensity (intensity being defined as the maximum sustained wind speed over the lifetime of a TC), respectively, in the Tonga region. The results are consistent with previous studies (e.g., Kimball and Mulekar, 2004; McInnes et al., 2014) with the radius of maximum winds increasing poleward (Fig. 2b) and decreasing with increasing intensity (Fig. 2c).

2.2. Oceanic Niño index (ONI)

The Oceanic Niño Index (ONI) is a metric to capture variations of SST anomalies in the Niño 3.4 region (5°N-5°S, 170°W-120°W) and provides information on the state of the ENSO. The ONI is calculated using a 3-month running mean of SST anomalies in the Niño 3.4 region over a 30-year (1986–2015) base period. A year is classified as El Niño (La Niña) when the ONI is $\geq +0.5$ °C (≤ -0.5 °C) for at least five consecutive overlapping 3-month seasons. An ENSO-neutral year is when the ONI is between the two thresholds. Using this definition, a total of 18, 19 and 13 El Niño, La Niña and ENSO-neutral events were obtained, respectively.

2.3. Tide gauge data

Tide gauge data for Nuku'alofa were obtained from the Australian Bureau of Meteorology (BOM)'s South Pacific Sea Level and Climate Monitoring Project website (http://www.bom.gov.au/pacificsealevel/). The dataset contains hourly readings of surface pressures, sea surface temperatures, surface air temperatures, sea level and wind speed and direction since January 1993. The tide gauge is part of a network of tide gauges in the South Pacific managed by the Bureau of Meteorology with monthly data reports about the oceanic and meteorological fields produced from these gauges available at the following website: http://www.bom.gov.au/oceanography/projects/spslcmp/data/monthly.shtml. While all efforts have been made to ensure the veracity of the tide gauge dataset, some limitations remain, for example, the tide gauge dataset may suffer from the vertical land motions which could result in either overestimating or underestimating the actual sea level height (Pfeffer et al., 2017).

The monthly sea level anomalies are obtained by removing the monthly climatology from the monthly means, which were computed from the hourly readings. The average monthly SST anomalies from July to June are used for the analysis, consistent with the TC season definition.

2.4. TC spatial distribution

The hexagonal gridding method, proximity method, and the Kernel Density Estimation (KDE) function are applied for spatial and temporal analysis of the distribution of TCs. We define "direct hit" when the centre of a TC passes within 1° (~100 km) of Nuku'alofa. This is when the inner circle of a TC (i.e., 1° radius from the centre of a TC; Weatherford and Gray, 1988), which consists of the strongest winds and maximum rainfall rate, is expected to affect Nuku'alofa. The main island is small relative to the size of an average storm, and so a TC centre need not necessarily pass over the land to have a significant impact on the lives and properties.

The hexagonal gridding method is used to aptly capture and grid TC tracks. The numbers of TC tracks transecting each hexagonal grid point are counted and then divided by the number of years to give spatial density (number of TCs per year). The grid radius of 1.5° has been chosen as it better represents spatial data distribution, especially in both data-dense and scarce areas.

The Kernel Density Estimation (KDE; Bowman and Azzalini, 1997) function is used to identify the spatial distribution of TCs genesis and decay points following Ramsay and Doswell, 2005, Ramsay et al. (2008), and Chand and Walsh (2009). Following Sharma et al. (2020), the TC genesis (decay) point is considered the first (last) coordinate in a track. KDE is also used to estimate characteristics and climatology of TC parameters such as central pressures, the direction of the entrance, translational speed and radius of maximum winds following McInnes et al. (2014).

KDE is a probability distribution function whereby a density function, the kernel, is used in a nonparametric manner to produce an estimation of the true density of the empirical distribution (Bowman and Azzalini, 1997). There exist numerous forms of Kernel functions, but we use here the Gaussian distribution given by Equation (3):

$$KDE = (1/nh)\sum_{i=1}^{n} K(x - x_i)/h \quad (3)$$

where K is the Kernel function, n is the number of intervals, and h is the bandwidth.

2.5. Accumulated cyclone energy

The accumulated cyclone energy (ACE; see Equation (4); Bell et al., 2000) is a useful index for measuring potential climatological trends (Chand et al., 2019) and is computed using the maximum wind speed measured at 6-h intervals over the entire time that the cyclone strength is at least 66 m/s (34 knots). Therefore, the ACE Index value depends on the intensity, frequency and duration of TCs in a given season. ACE has been used in several studies to summarise TC activity for the season or examine past TC activities (e.g., Bell et al., 2000; Camargo and Sobel, 2005; Chand and Walsh, 2009; Villarini and Vecchi, 2012; Hartfield et al., 2018; Blunden and Arndt, 2019).

$$ACE = \sum_{i=1}^{N}\sum_{n=1}^{M_i} V_{i,n}^2 \quad (4)$$

where V is the 6-hourly maximum wind speed in m/s (with values of at least 66 m/s), $i = 1,..,N$ is the set of N number of TCs, M_i is the set of M numbers of times the 6-hourly V exceed 66 m/s.

3. Results and discussions

3.1. Climatology, seasonality, and variability of TCs

A total of 128 TCs (~2.6 TCs per year) were observed in the Tonga region over the 1970–2019 period. Of these, 49 TCs occurred in the 19 La Niña years (~2.6 TCs per La Niña year), 49 TCs occurred during 18 El Niño years (~2.9 TCs per El Niño year) and 30 TCs were identified in 13 ENSO-neutral years (i.e., ~2.3 TCs per ENSO-neutral year). Although the average number of TCs during El Niño is relatively higher than La Niña, their relationship is not systematic, for example, 0 TCs occur during the 1992 El Niño but 5 TCs during the 2003 La Niña. This also shows that the annual numbers of TCs are highly variable from one year to another. However, it should be noted that the differences between the average TCs during El Niño, La Niña and Neutral years were found to be statistically insignificant (i.e., all p-values > 0.05 using a student's t-test).

The closeness in the annual average numbers of TCs during El Niño and La Niña for the Tonga region implies that the Tonga region lies in a neutral ground similar to the Fiji region as found by Kostaschuk et al. (2001) where the impact of ENSO on the frequency of TCs is weak. Similar results were obtained by Basher and Zheng. (1995) and Chand and Walsh (2009) for the FST region. However, comparing the annual

average frequency of TCs alone is not enough to explain the extent of the impact of ENSO on TCs affecting the Tonga region. Consequently, here we investigate to what extent the influence of ENSO has upon other characteristics of TC activities affecting the Tonga region.

TCs mainly occur in the Tonga region during November to April (Fig. 3), although some TCs can also occur outside of the season often associated with the early onset of ENSO events (e.g., Chand and Walsh, 2009). Climatologically, most TCs have occurred from January to March, with January having the highest proportion (26.9%), followed by February (23.1%) and March (16.7%) when the local SST is warmest (see Fig 14.2 in Australian Bureau of Meteorology and CSIRO, 2011). In the wider SWP region, January and February are the dominant months for TCs with February having the highest proportion (Terry, 2007).

The proportion for the rest of the months during the TC seasons are 15.7% for December, 1.9% for November, and 12.0% for April. A total of 3.7% of TCs occurred outside of the TC season with 1.9% in May and 0.9% each for July and October. Fig. 3 also demonstrates that January and February have the highest occurrence of the number of severe TCs (or hurricanes) with 0.20 TCs per month, followed by 0.18 TCs each for March and December, 0.06 TCs for April, and 0.02 TCs each for October and November. In any year, the proportion of TCs in the hurricane intensity (Categories 3, 4 and 5) is ~38.8%, storm intensity (Category 2) is ~22.5%, gale intensity (Category 1) is ~31.5%, and ~7.2% of tropical depressions (TDs) observed in the region.

3.1.1. *Spatial distributions of TC track, genesis, maximum intensity and decay*

TC track spatial density (TCs per year) has been measured using hexagonal grids (Fig. 4). The climatological TC track spatial density for each grid that lies inside the Tonga region varies between 0.10 and 0.50 TCs per year, with relatively higher density observed during El Niño (0.05–0.85 TCs per year) than La Niña (0.04–0.67 TCs per year) or ENSO-neutral years (0.07–0.46 TCs per year).

During La Niña, the spatial variability is low. In contrast, during El Niño, where the spatial variability is large, some areas are more vulnerable than others. However, in the northwest and southwest quadrants including Nuku'alofa, variability is less but the risk is quite high relative to other quadrants. This indicates Nuku'alofa has a high risk of being affected by the left side of the TC with respect to the system motion, where rainfall is maximum (Villarini et al., 2011) and winds are strongest because of the translation speed of the system contributing to the winds of the TC. These strong winds often lead to sea flooding, especially when coinciding with high tide (Terry, 2007). Fig. 4 also generally shows TCs clustered immediately to the northwest and southwest of the Tonga region implying most TCs entered from the northwest and exited to the southeast of the region.

TC genesis points with contours enclosing areas representative of 25%, 50% and 75% of the total population affecting the Tonga region using the KDE function are shown in Fig. 5. The contours of TC genesis for all years (Fig. 5a) show that the Tonga region is most vulnerable to TC formed in the area between 7°S and 19°S, and 162°E and 192°E, which is equivalent to about 75% of the overall genesis with the highest density centred around 14°S, 183°E (or ~800 km northwest of Nuku'alofa).

During El Niño years (Fig. 5b), the SPCZ shifts northeastward and away from the Tonga region. Consequently, the TC genesis density centre shifts northwestward and away from Nuku'alofa to around 12.5°S, 179.2°E underneath the area where the favourable low-level vorticity, upper-level divergence and vertical wind shear coincide (see Fig. 8a1&a2 and Fig. 9a in Chand and Walsh, 2009), contrary to the northeastward shift of the main density of TC genesis during El Niño in the FST region (Chand and Walsh, 2009) and in the SWP (Hastings, 1990; Chu, 2004; Terry, 2007; Kuleshov et al., 2008; Terry and Gienko, 2010; Vincent et al., 2011; Dowdy et al., 2012; Iizuka and Matsuura, 2012; Chand et al., 2013; Diamond et al., 2013, 2015; Brown et al., 2020; Sharma et al., 2020). This result has important implications for seasonal and climatological predictions of TCs at island scales and it highlights the importance of TC tracks and their associated steering mechanisms. However, as with many other earlier studies (e.g., Chand and Walsh, 2009; Dowdy et al., 2012; Ramsay et al., 2012; Chand et al., 2020), this study concurs that TC genesis shifts equatorward during El Niño years. The TC genesis density centre lying to the west of the date line and north of 15°S during El Niño indicates that the predominant wind steering regime is the upper-level westerly winds (mid-level southeastward winds) steering TCs towards the northern part of Fiji and the Tonga region in the FST region (see Fig. 10a1&b1 in Chand and Walsh, 2009; directions in which these TCs entered the Tonga region is discussed later in section 3.1.2).

During La Niña years (Fig. 5c), the SPCZ shifts southwestward and closer to the Tonga region. Consequently, the maximum density of TC genesis shifts southwestward by about 100 km relative to climatology to around 15.3°S, 181.4°E and again underneath an area where favourable

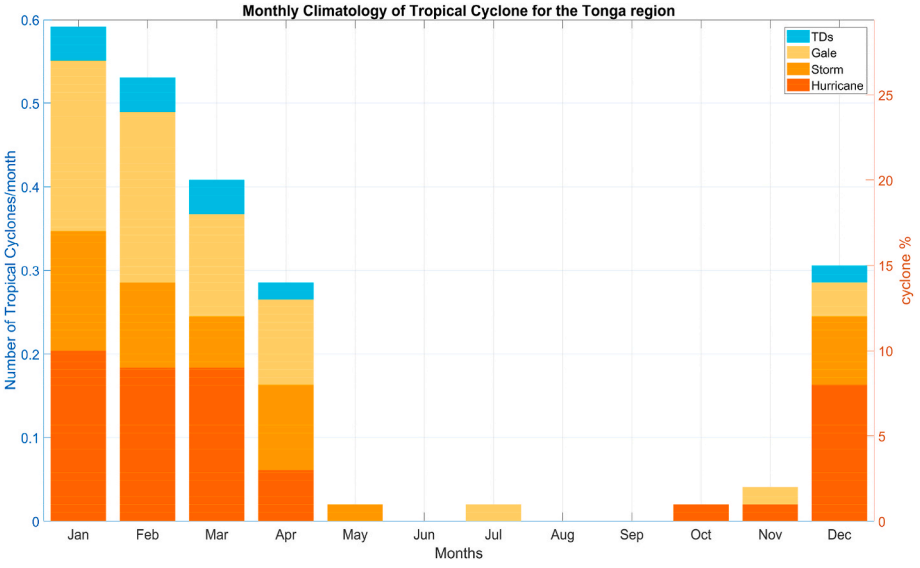

Fig. 3. Averaged number of TCs transecting the Tonga region per month between 1970 and 2019. TCs are categorised into TDs (in cyan), Gale (light orange; Category 1), Storm (orange; Category 2), and Hurricane (dark orange; Categories 3, 4 and 5). (For interpretation of the references to colour in this figure legend, the reader is referred to the Web version of this article.)

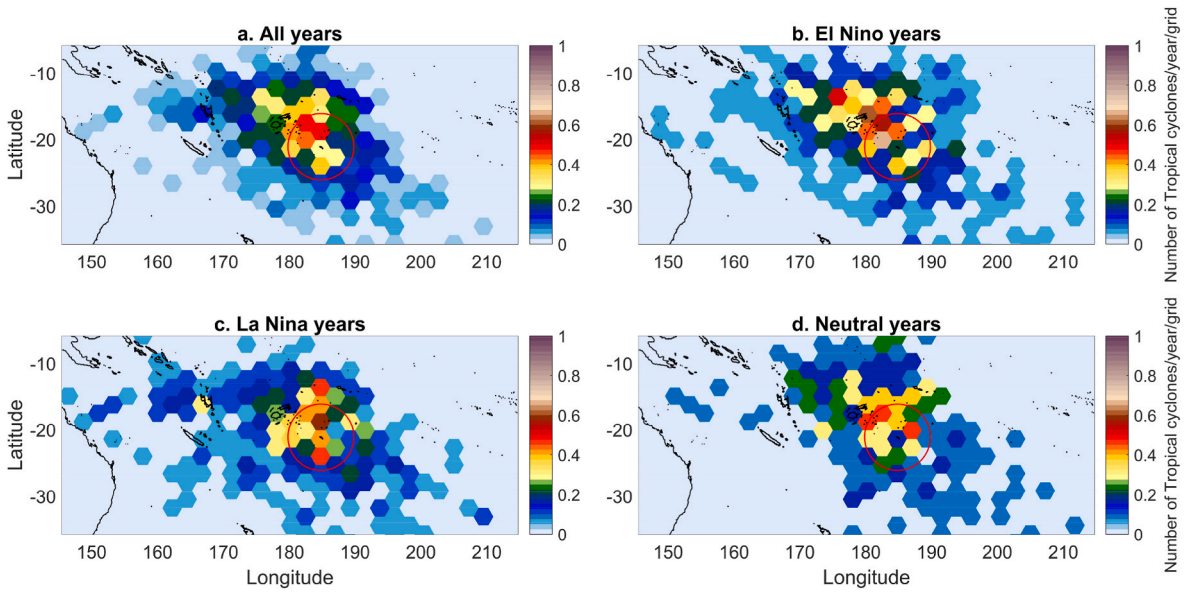

Fig. 4. Spatial distributions of the average number of TCs per year for (a) all years, (b) El Niño years, (c) La Niña years and d) ENSO-neutral years transecting the Tonga region between 1970 and 2019. The red circle is centred on Nuku'alofa, Tongatapu. (For interpretation of the references to colour in this figure legend, the reader is referred to the Web version of this article.)

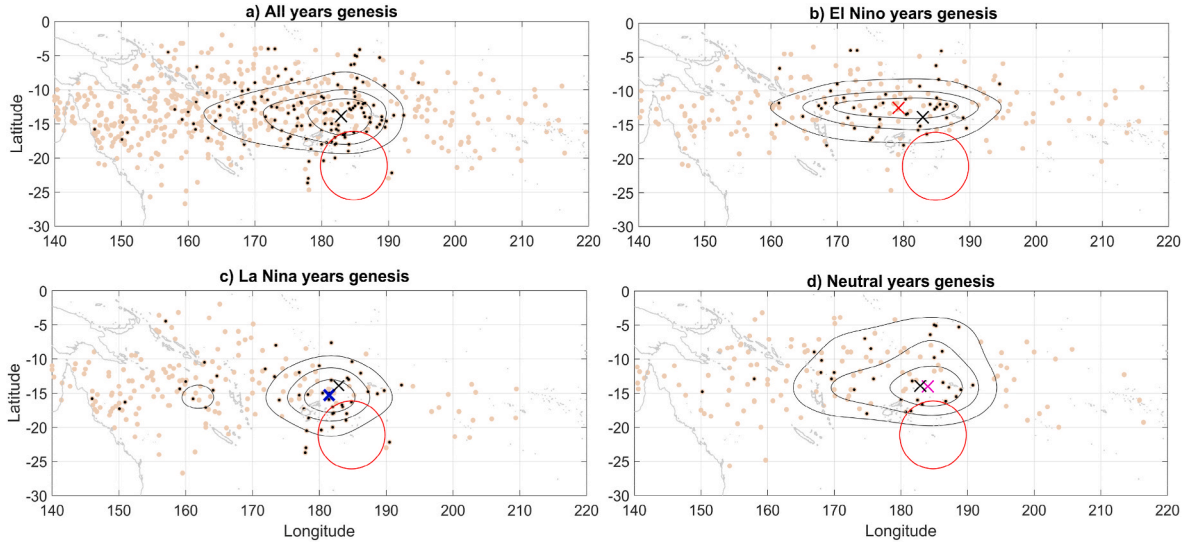

Fig. 5. Location of TC genesis points affecting Tonga (black dots) and the SWP (orange dots) for (a) all years, (b) El Niño years, (c) La Niña years and (d) ENSO-neutral years. Contours enclose areas within which TC genesis have 25%, 50%, and 75% probabilities of occurrence given by the KDE function. The TC density centres are represented by X in black for climatology (for all plots), in red for El Niño (b), in blue for La Niña (c), and in magenta for ENSO-neutral years (d). (For interpretation of the references to colour in this figure legend, the reader is referred to the Web version of this article.)

low-level vorticity, upper divergence and vertical wind shear coincide in the FST region (see Fig. 8b1&b2 and Fig. 9b in Chand and Walsh, 2009) but to the south of the large-scale favourable environment during El Niño. This southwestward shift makes it consistent with earlier studies (e.g., Hastings, 1990; Chu, 2004; Terry, 2007; Kuleshov et al., 2008; Terry and Gienko, 2010; Dowdy et al., 2012; Iizuka and Matsuura, 2012; Chand et al., 2013; Diamond et al., 2013; Sharma et al., 2020), and thus doubling the chance of TCs forming inside the Tonga region from 10% during El Niño to 20.4% during La Niña. Both the doubling in the chance of TC formation within the Tonga region and the favourable mid-level southeastward steering wind aloft during La Niña (Chand and Walsh, 2009) may explain why the average annual number of TCs during La Niña is also high and comparable to El Niño and larger than ENSO-neutral.

During ENSO-neutral years (Fig. 5d), the SPCZ lies between the mean positions of the SPCZ during El Niño (to the north) and La Niña (to the south) (Vincent et al., 2011). As a result, the main density centre shifts eastward by about 100 km relative to climatology, lying directly to the north of Nuku'alofa. The contours of TC genesis span a relatively larger area meridionally (4°-20°S), including more than a quarter of the Tonga region and accounting for 2% of genesis points. Aloft in this area of maximum density centre lies the favourable large-scale environment such as low-level vorticity, upper-level divergence and vertical wind shear (see Fig. 8c1&c2 and Fig. 9c in Chand and Walsh, 2009). This density centre sitting directly to the north of Nuku'alofa is consistent with previous studies showing that the meridional component of TC movements particularly east of the date line in the FST region is dominant during ENSO-neutral years (see Fig 11 in Chand and Walsh, 2009).

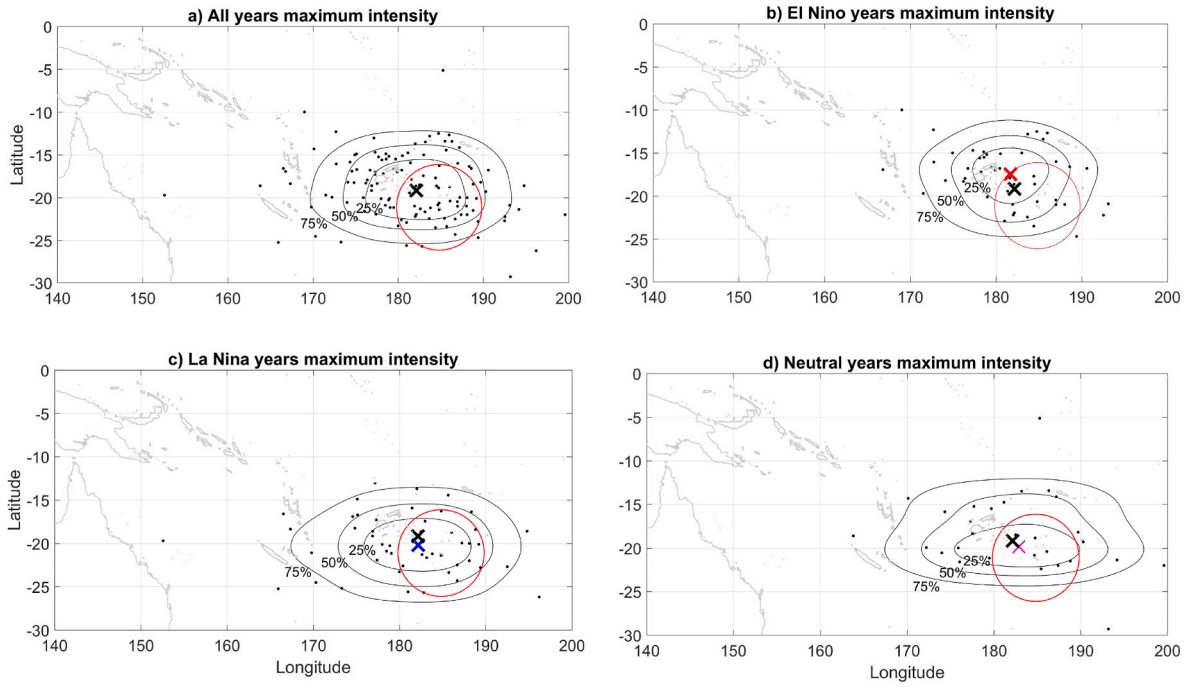

Fig. 6. Distributions of maximum intensity of TCs affecting Tonga during (a) all years, (b) El Niño, (c) La Niña and (d) ENSO-neutral given by the KDE function. The TC density centres of maximum winds are represented by X in black for climatology (for all plots), in red for El Niño (b), in blue for La Niña (c) and, in magenta for ENSO-neutral years (d). (For interpretation of the references to colour in this figure legend, the reader is referred to the Web version of this article.)

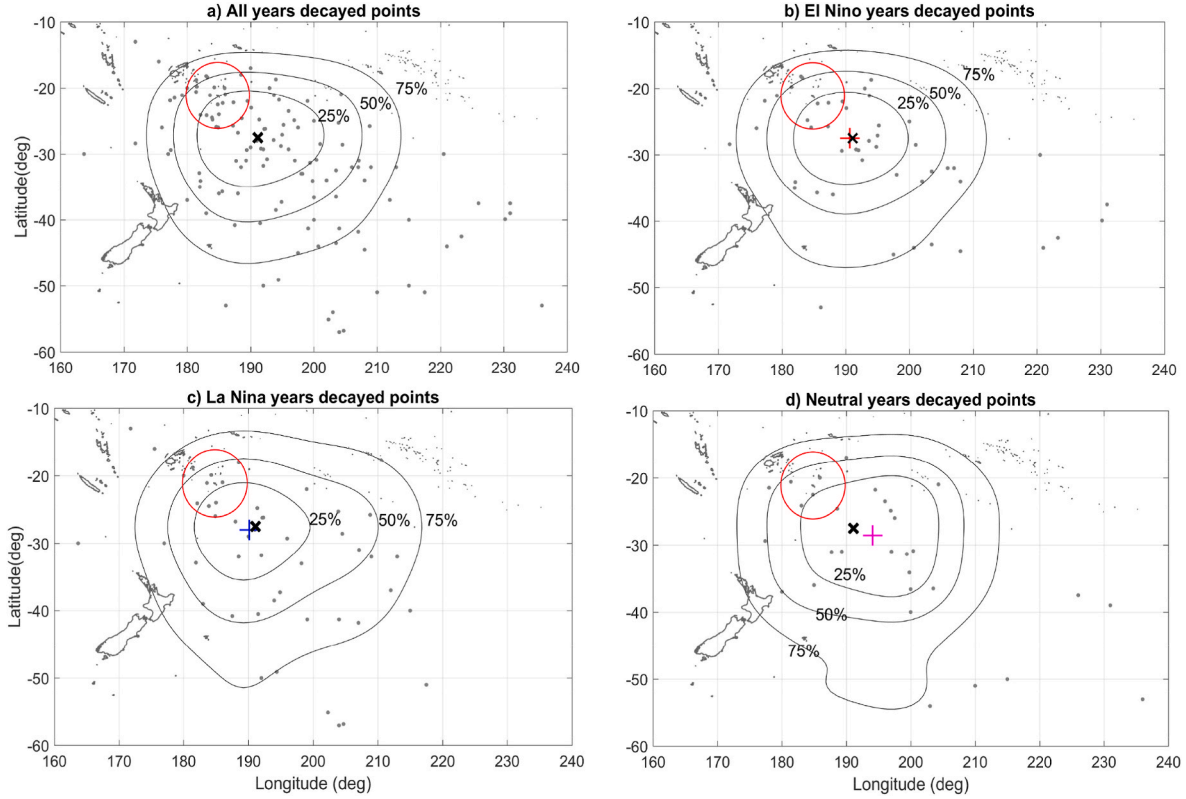

Fig. 7. Decay points of TCs that affected the Tonga region. Contours enclose areas within which TC decay points had 25%, 50%, and 75% given by the KDEs. The TC decay density centre is represented by X in black for climatology (for all plots), + in red for El Niño (b), + in blue for La Niña (c) and + in magenta for ENSO-neutral years (d). (For interpretation of the references to colour in this figure legend, the reader is referred to the Web version of this article.)

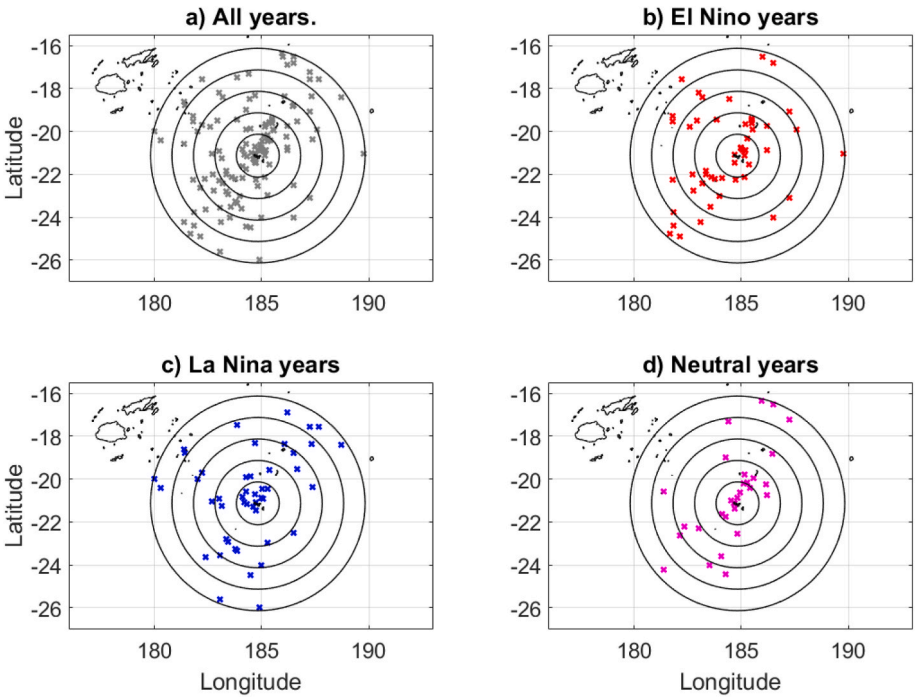

Fig. 8. Observed TCs at their closest distance to Nuku'alofa during (a) all years, (b) El Niño years, (c) La Niña years and (d) ENSO-neutral years for the period 1979–2019. The concentric circles are centred on Nuku'alofa and the radial distance between each circle is 1°. (For interpretation of the references to colour in this figure legend, the reader is referred to the Web version of this article.)

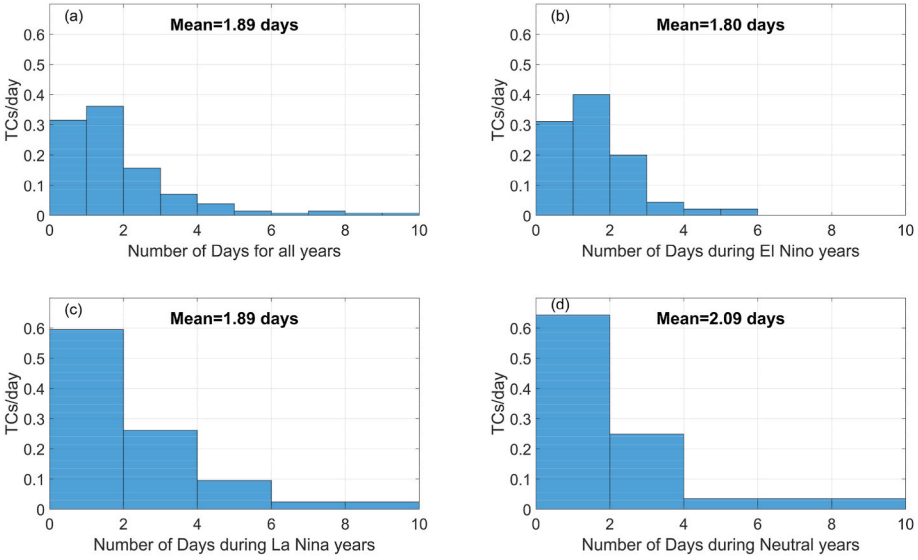

Fig. 9. TCs lifetime in the number of days for (a) all years, (b) El Niño years, (c) La Niña years and (d) ENSO-neutral years in the Tonga region between 1970 and 2019.

In the SWP, TC tracks have been categorised into 4 types according to their sinuosity: straight, quasi-straight, curving and sinuous (Terry and Gienko, 2010). The most dominant type, which has its genesis between 160°E and 180°E, is the sinuous category accounting for one-third of all tracks within 160°–180°E, a favourable place especially during El Niño years for TCs affecting the Tonga region are formed (Fig. 5). The sinuous category poses a higher risk to Tonga as they tend to have greater life-spans and intensity. Recent instances are TC Gita from 1 to 22 February 2018 and TC Ian from 4 to 15 January 2014, with both of category 5 intensity when they passed the Tonga region.

The maximum TC intensity distribution with contours enclosing 25%, 50% and 75% of the total number of TCs as determined using the KDE function is shown in Fig. 6. The latitudinal variations for all years (climatology; Fig. 6a), La Niña (Fig. 6c) and ENSO-neutral (Fig. 6d) of the annual average of TC intensity show a strong symmetry across 20°S, but further north across 17°S during El Niño (Fig. 6b). The spatial distribution of the maximum TC intensity seems to occur in a fairly zonal pattern, with the ratio of longitudes to latitudes of the 75% contour, for example, higher during La Niña (2.3) than El Niño (1.7) with the largest during ENSO-neutral years (2.5). This shows that during El Niño, TCs reach their maximum intensity relatively closer to the Tonga region, compared to La Niña and ENSO-neutral. The climatological maximum density centre lies inside the Tonga region, about 350 km northwest of Nuku'alofa, shifting northward during El Niño by ~190 km, southward

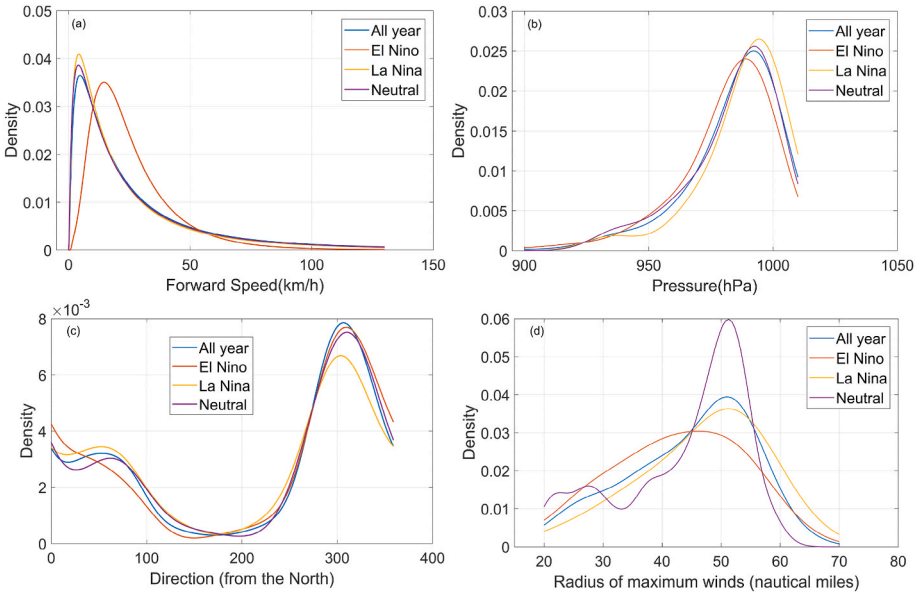

Fig. 10. Probability density function of TCs (a) forward speed, (b) minimum pressures, (c) direction of entrance from North, and (d) radius of maximum winds of observed TCs in the Tonga region during all years (in blue), El Niño (in red), La Niña years (in yellow) and ENSO-neutral years (in purple). (For interpretation of the references to colour in this figure legend, the reader is referred to the Web version of this article.)

by ~120 km during La Niña and southeastward by ~100 km during ENSO-neutral years relative to climatology. Generally, TCs tend to intensify as they move poleward and reach maximum intensity earlier during El Niño when compared to La Niña and ENSO-neutral years. This is consistent with earlier studies (e.g., Sinclair, 2002; Chand and Walsh, 2011; Dowdy et al., 2012) because the large-scale environmental variables conducive for intensification equatorward of 15°S in the FST region is more favourable during El Niño than during La Niña (Chand and Walsh, 2010).

The TC decay distribution with contours of 25%, 50% and 75% representative of the total number of TCs using the KDE function is shown in Fig. 7. Generally, TCs tend to weaken as they encounter unfavourable large-scale environmental variables (i.e., cooler sea surface temperatures and enhanced upper-level westerlies winds) as they move towards higher latitudes (Sinclair, 2002; Dowdy et al., 2012). The TC decay points may reflect where they come from, how fast they move and the state of the ENSO. The majority of the decay points are to the southeast of the Tonga region indicating that these TCs were influenced by the upper-level westerlies (mid-level southeastward steering wind) as they moved poleward. The main density centres for climatology and El Niño lie relatively close to each other at around 27.5°S, 191.1°E and 27.4°S, 190.6°E, respectively or ~50 km apart. Whereas during La Niña (ENSO-neutral), the density centre is about 115 km (315 km) southwest (southeast) of the climatology. The 75% contour coverage is extended relatively more poleward and eastward during La Niña and ENSO-neutral years than during El Niño. This indicates that the meridional component of the upper-level westerlies is more dominant during El Niño, compared to its counterparts, while the zonal component is more dominant during La Niña and ENSO-neutral years as they encounter higher latitudes. This is in contrast with the findings for TC tracks east of New Zealand in which the zonal component is dominant during El Niño years and the meridional component during La Niña (Sinclair, 2002). This may be due to TCs formed in the west during La Niña being steered by the upper-level westerlies towards the Tonga region (Chand and Walsh, 2010) with a more zonal component, while during El Niño, TC genesis occurs to the northwest of the region and TCs are tracked southeastwards with a strong meridional component.

The chance of TCs terminating inside the region is 10.8%, relatively higher during El Niño with 14.6%, 13.3% during ENSO-neutral years, and 4.1% during La Niña. During El Niño, the density centre is located equatorward of climatology and its counterparts indicating that TC's lifetime during El Niño years is relatively shorter (Sinclair, 2002; Chand et al., 2013). This is possibly due to the large-scale atmospheric conditions favourable for intensification being diminished rapidly by 15°S in the FST subregion, especially during El Niño (Chand and Walsh, 2011).

3.1.2. Other TC parameters: Closest distance, TC days, direction of entrance, central pressure, translation speed, and radius of maximum winds

The closest distance of all TCs to Nuku'alofa overlaid with 1°, 2°, 3°, 4° and 5° radii circles centred on Nuku'alofa is shown in Fig. 8. The mean climatology of the closest distance of TCs to Nuku'alofa is ~2.3°; about 2.3°, 2.5° and 2.0° during El Niño, La Niña and ENSO-neutral years, respectively. The mean climatology distribution indicates that about 50% of TCs lie within 2° radii. Fig. 8 also shows the risk of a "direct hit" (i.e., the centre of TC passing within a 1° radius of Nuku'alofa) in Tonga in any year with a climatological mean of ~0.6 TCs per year, ~0.5 TCs during El Niño, ~0.6 TCs during La Niña, and ~0.7 TCs during ENSO-neutral years. In general, regardless of the stage of the ENSO, Nuku'alofa is expected to experience a direct hit of at least one TC every year and this has implications for seasonal and climatological forecasting for Tonga.

The mean climatology of the number of TC days is ~8 days from genesis to decay. The number of TC days per year within the Tonga region is shown in Fig. 9. The mean climatology of the number of TC days per year is 1.9. During La Niña years, TCs appear to spend a longer period within the Tonga region with an average of 3.4 days, 2.1 days during ENSO-neutral and shortest during El Niño with 1.7 days. These values are dependent on the mid-level southeastward steering winds aloft (or upper-level westerlies; Sinclair, 2002; Terry, 2007; Chand and Walsh, 2009), which are greater during El Niño (Sinclair, 2002; Dowdy et al., 2012).

The mean climatology of the translational speed of TCs within the Tonga region is 18.9 km/h (Fig. 10a). Relative to the mean climatology, TCs are moving faster during El Niño and ENSO-neutral years at 23.8 km/h and 20.0 km/h, respectively, and a little slower at 19.1 km/h during La Niña (Fig. 10). This is also consistent with Fig. 9 which shows that the number of days during El Niño is relatively smaller as opposed to the number of days during La Niña and ENSO-neutral years inside the Tonga region. This is because the mid-level southeastward steering wind, which is mostly responsible for steering TCs in this area (Sinclair,

2002; Terry, 2007; Ramsay et al., 2012), is stronger during El Niño years (Sinclair, 2002; Terry, 2007; Chand and Walsh, 2010; Dowdy et al., 2012; Chand et al., 2020). Consistent with this finding, TC tracks east of 170°E can be represented by a single and relatively straight northwest-southeast track reminiscent of the mid-level southeastward steering wind aloft (see Fig. 2 in Ramsay et al., 2012). However, other dynamical steering mechanisms are the beta effect (Chan and Williams, 1987) and the subtropical ridge (Terry, 2007), usually dominant during the early stages of TC lifetime especially north of 15°S and east of 160°E in the SWP, transporting TCs generally southwestward before being recurved by the dominant southeastward steering winds poleward of ~15°S (see Fig. 2a, b and c in Dowdy et al., 2012). Nevertheless, only a small fraction of the overall TC tracks east of 170°E are following this recurvature when compared to the majority of the tracks (Ramsay et al., 2012). In contrast, TC track recurvature is a major characteristic of TCs in the Western North Pacific (Camargo et al., 2007).

During La Niña, the mid-level southeastward steering wind is displaced poleward allowing the subtropical ridge and beta effect to become dominant and steering TCs, with origins north of Tonga, to the south and southwest, while the majority which lies to the west and northwest is steered by this southeastward steering wind towards the Tonga region (see Fig. 2c in Dowdy et al., 2012).

The mean climatological pressure of TCs inside the Tonga region is 984.0 hPa (Fig. 10b). TCs are relatively stronger during El Niño (~981.1 hPa) than during La Niña (~987.9 hPa) and ENSO-neutral years (~983.0 hPa), consistent with previous studies (e.g., Chand and Walsh, 2009; Kuleshov et al., 2009; Dowdy et al., 2012). More (less) intense TCs are formed during El Niño (La Niña) due to higher (lower) surface temperatures and the enhanced (suppressed) convective activities in the eastern Equatorial Pacific resulting from the northeastward (southwestward) movement of the SPCZ (Kuleshov et al., 2009; Vincent et al., 2011).

The preferred direction of the entrance is from the northwest regardless of the phases of the ENSO and the variations between them are small (Fig. 10c). The mean climatology is 331.9°, 329.7° during El Niño, 334.3° during La Niña and 332.2° during ENSO-neutral years. This is consistent with Fig. 4, which means the Tongan region lies in an area where TCs formed to the west and northwest are steered by the mid-level southeastward steering winds into the area (Chand and Walsh, 2009).

The size of TCs is also affected by ENSO. The radius of maximum winds relative to the climatology is relatively skewed to smaller (larger) values during El Niño (La Niña) (Fig. 10d) but confined to the interval 45–55 nm, with a few outliers during ENSO-neutral years. This implies that TCs are relatively smaller during El Niño, larger during La Niña and close to climatology during ENSO-neutral years. TC sizes are consistent with Fig. 10b as TCs are relatively stronger (weaker) during El Niño (La Niña) years, hence their sizes, in theory, are expected to be smaller (larger) (Knaff et al., 2016).

3.2. TC trends and correlations

The trend for the number of TCs affecting the region is decreasing at a rate of 0.0225 TCs per year. However, the trend for the number of severe TCs (hurricanes) is increasing at a rate of 0.0095 TCs per year (not shown). Both trends are not significantly different from zero (i.e., the null hypothesis being that there is no trend) from a student's t-test (p-value = 0.177 for the number of TCs and 0.259 for the number of severe TCs). These trends are consistent with previous studies (e.g., Tauvale and Tsuboki, 2019) in that the occurrence of stronger TCs in other regions of the SWP is increasing while the overall TCs per year is decreasing. In contrast, Kuleshov et al. (2020) found a decreasing trend for the overall number of TCs as well as the number of severe TCs in the SWP highlighting the challenge of detecting any signal due to anthropogenic-induced climate change from a relatively short period of record.

Similar trends in the overall number of TCs in the Tonga region have been found during El Niño years though not statistically significant (p-value = 0.989 for the number of TCs and 0.168 for the number of severe TCs). The trend for the number of TCs per year is decreasing at a rate of 0.0002 while the trend for the number of severe TCs is increasing at a higher rate of 0.0103 TCs per year compared to climatology.

Similarly, during La Niña years, the trend for the number of TCs per year is decreasing at a rate of 0.0095 TCs per year (p-value = 0.557), while the trend for the number of severe TCs per year is increasing at 0.0026 TCs per year (p-value = 0.637), at a lower rate than during El Niño years. A decreasing trend in ENSO-neutral years has been obtained both for all TCs and severe TCs at a rate of 0.0128 and 0.0011 TCs per year, respectively, which are not significantly different from zero (p-values of 0.312 for the former and 0.826 for the latter).

This decreasing trend in the overall TCs, and during ENSO, may be explained from different perspectives. First, it can be explained by the increase in upper atmospheric stability due to warmer air in the upper atmosphere in comparison to the lower atmosphere preventing TC formations as found by Maru et al. (2018) for the Solomon Islands. Second, the northeastward decadal shift in the density of TC genesis in the SWP towards central Pacific (Sharma et al., 2020) may have an implication on the decadal climatological steering flow resulting in some areas like Tonga being deprived of TC activity. Moreover, the large temporal variability of TC activity may result in this decreasing but not significant trend (Chan, 2006).

In contrast, the increasing trend of severe TCs may also be accounted for by the change in analytical practices that may have contributed to some extent. The application of the Dvorak technique, a satellite-based tool for analysing the intensity of TCs starting in the early 1970s (Dvorak, 1973, 1975) was first introduced in the late 1970s at the World Meteorological Organisation (WMO) regional centre in Fiji, which is responsible for providing warnings for the area 0–25°S, 160°E–240°E in the SWP (Terry and Gienko, 2010), but with low-resolution imagery. However, only when the high-resolution imageries became available in the early 1990s, did the technique become increasingly used and mastered competently by forecasters in Fiji indicating that earlier records of TC intensity with central pressure less than 950 hPa were likely to be underestimated (Kuleshov et al., 2010). Nevertheless, TCs with severe strength would be hard to miss, although with low-resolution satellite imagery due to their potential devastative threat and generally longer lifetime than relatively weaker TCs (Terry and Gienko, 2010).

The ACE for TCs affecting the Tonga region is highly variable from one year to another and its trend is decreasing at a rate of 0.0005 TCs per year, though not statistically significant (p-value = 0.806). This decreasing trend together with the decreasing trend in the overall number of TCs implies that the TC frequency may be dominating the ACE as opposed to combining the mean intensity and length of TC days. This decreasing trend of ACE aligns with previous findings that the area of study (the Tonga region) lies poleward of 15°S, an area not favourable for high values of ACE in the FST region (Chand and Walsh, 2011).

An analysis of the linear relationship between the number of TCs and severe TCs with ENSO, local sea level (SL), and local SST anomalies revealed weak and non-significant correlations (at the 95% confidence level). This is consistent with the finding of Basher and Zheng (1995) that the region containing Tonga and Fiji is weakly correlated to ENSO and SST indicating large-scale atmospheric conditions are responsible for TC genesis in this area.

4. Conclusions

The SPEArTC dataset that contains TC best track information has been used to construct climatological means, variability and trends of TCs passing within a 500 km radius of Nuku'alofa, Tonga, at the country scale. Climatological states of various characteristics of TCs were analysed and compared with those associated with different ENSO phases (El Niño, La Niña, ENSO-neutral phase).

A total of 128 tracks formed within (10%) or entered the Tongan region over the 1970–2019 period. Generally, a seasonal average of ~2.6 TCs is expected, half of which occur in January and February, and ~38.8% are categorised as hurricanes (or severe TCs). Relatively more (less) TCs occur during El Niño (La Niña) years with an average of ~2.9 (~2.6) TCs per year and both are greater than TCs occurring during ENSO-neutral years (~2.3 TCs per year), however, these differences are insignificant.

The Tonga region lies in an area that is affected by the SPCZ, where within 10° poleward of its mean axis is the incubation zone of TC formation, which in turn modulated by ENSO. During El Niño (La Niña) years, the SPCZ moves northeastward (southwestward) and away from (closer to) Tonga. Consequently, TC genesis affecting the Tonga region tends to shift northwestward (southwestward) and away from [Fig. 5b] (towards [Fig. 5c]) the Tonga region. Despite that, 10% (20%) of the TC genesis occurs inside the Tonga region.

At the early stage of their lifetime, TCs undergo poleward-motion due to the beta effect and the subtropical ridge at lower latitudes. Subsequently, they tend to undertake southeastward-motion due to encountering the upper-level westerlies while intensifying and reaching their maximum strength relatively more equatorward [Fig. 6b] (poleward [Fig. 6c]) with higher (lower) intensity [Fig. 10b] and smaller (larger) TC size [Fig. 10d]. They enter the Tonga region from the northwest at 329.7° (334.3°) [Fig. 10c] with higher (lower) southeastward steering wind may lead to a faster (slower) translation speed [Fig. 10a] and a lower [Fig. 9b] (higher [Fig. 9c]) number of TC days and passing closer to [Fig. 8b] (further away from [Fig. 8c]) Nuku'alofa. Upon entering the southern half of the Tonga region, TCs decay early [Fig. 7b] (late [Fig. 7c]) due to encountering earlier (later) cooler sea surface temperatures and stronger upper-level westerlies as they move poleward with a lower (larger) zonal component.

An investigation into how ENSO and local SST influence TCs affecting the Tonga region shows no significant statistical linear relations. Analysing ACE as an index associated with the combination of the frequency of TCs, length of TC days and intensity show a decreasing trend indicating that the frequency of TCs seems to be the primary contributor, however, the trend was not statistically significant.

With the impact of anthropogenic climate change, decreasing and increasing trends in the overall number of TCs and severe TCs, respectively, have been identified. However, detecting changes due to natural variability or climate change is a challenge due to the short historical records. In addition, the change in the forecasting system and low-resolution satellite imagery, especially in the early period of this data may have also raised doubt about the accuracy of the historical record especially in categorizing the intensity of TCs.

The gap in average numbers of TCs between El Niño and La Niña found in this study would be increasing in the future when more extreme El Niño years than La Niña are anticipated (e.g., Wang et al., 2019). In addition, if the decreasing trend of the overall number of TCs together with the increasing trend of severe TCs affecting the Tonga region continues and becomes statistically significant, it implies fewer but more severe TCs and thus more devastating due to their severity, slow translation speed, prolonged lifetime, and poleward migratory.

While general agreements on the characteristics of TCs in the regional scale were found during ENSO, a few notable significant differences were also found specific to the Tonga region at the country level, when TC years were grouped into ENSO phases. These are listed below.

- TC genesis is formed mostly between 7°S and 20°S, 160°E and 190°E, shifting northwest (southwest) during El Niño (La Niña) making the Tonga region more vulnerable especially during El Niño due to the sinuous category that tends to have greater lifespans and intensity.
- TC maximum intensity mostly occurred between 12°S and 25°S, 170°E and 196°E slightly shifting equatorward relative to climatology during El Niño, poleward during La Niña and eastward during ENSO-neutral years. This study shows the majority of TCs reach their maximum intensity earlier and closer to the Tonga region during El Niño, compared to their counterparts during other phases of ENSO.
- A direct hit on Nuku'alofa (i.e., the centre of TCs passes within a 1° radius of Nuku'alofa) is expected every year regardless of the phases of the ENSO, relatively higher during La Niña and ENSO-neutral years than during El Niño years.
- TCs are stronger, more frequent and have greater translational speed, shorter TC days, smaller size and closer distance to Nuku'alofa during El Niño years. In addition, Nuku'alofa lies to the left of most TCs with respect to the system motion where winds are strongest, rainfall is maximum, and the risk of sea flooding is highest. This implies the risk of damage during El Niño is higher as opposed to La Niña and ENSO-neutral years.
- During La Niña years, the chance of TC genesis in the Tonga region is doubled and TCs formed to the west are steered by the upper-level westerlies towards the Tonga region. These results can explain why the Tonga region are still affected by TCs during La Niña years.

Finally, traditional ENSO is not the only mode of climate variability that influence TC behaviour in SWP. Other modes of climate variabilities such as different ENSO types (e.g., Wang and Wang, 2013), Interdecadal Pacific Oscillation (Magee et al., 2017), Southern Annular Mode (Diamond and Renwick, 2015) and Indian Ocean SST variability (Magee and Verdon-Kidd, 2018) provide different effects on TC activity in SWP in general and Tonga in particular and could form a subject for further investigation.

Funding

The first author was supported by the Pacific Excellence in Research and Innovation (PERSI) scholarship from The University of the South Pacific.

Declaration of competing interest

The authors declare that they have no known competing financial interests or personal relationships that could have appeared to influence the work reported in this paper.

Acknowledgement

We acknowledge the Climate and Ocean Support Program in the Pacific (COSPPac) project for funding the publication of this manuscript.

Appendix

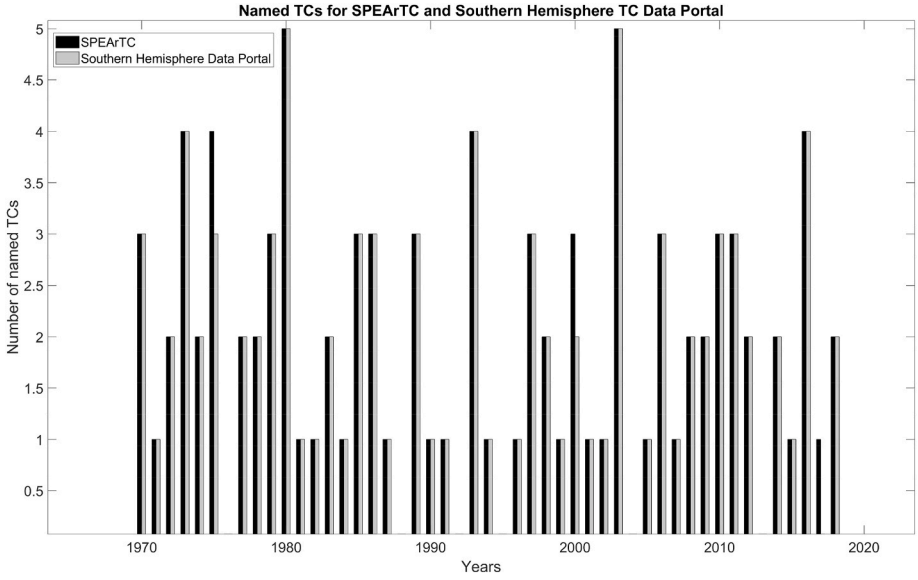

Fig. A1. Number of named TCs in the SPEArTC dataset (in black) and the number of named TCs in the Southern Hemisphere TCs Data Portal (in grey) that have been recorded to pass within 500 km of Nuku'alofa between 1970 and 2019.

References

Australian Bureau of Meteorology and CSIRO, 2011. Climate change in the pacific: scientific assessment and new Research. Countr. Rep. 2, 215–228 [Available online at. https://www.pacificclimatechangescience.org/publications/reports/report-climate-change-in-the-pacific-scientific-assessment-and-new-research/.

Basher, R.E., Zheng, X., 1995. Tropical cyclones in the southwest Pacific: spatial patterns and relationships to Southern Oscillation and sea surface temperature. J. Clim. 8 (5), 1249–1260. https://doi.org/10.1175/1520-0442(1995)008<1249:TCITSP>2.0.CO;2.

Bell, G.D., Halpert, M.S., Schnell, R.C., Higgins, R.W., Lawrimore, J., Kousky, V.E., Tinker, R., Thiaw, W., Chelliah, M., Artusa, A., 2000. Climate assessment for 1999. Bull. Am. Meteorol. Soc. 81 (6), S1–S50. Retrieved Dec 16, 2021, from. https://journals.ametsoc.org/view/journals/bams/81/6/1520-0477_2000_81_s1_caf_2_0_co_2.xml.

Blunden, J., Arndt, D.S., 2019. State of the climate in 2018. Bull. Am. Meteorol. Soc. 100 (9), Si–S306. https://doi.org/10.1175/2019BAMSStateoftheClimate.1.

Bowman, A.W., Azzalini, A., 1997. Applied Smoothing Techniques for Data Analysis: the Kernel Approach with S-Plus Illustrations, 18. OUP Oxford.

Brown, J.R., Lengaigne, M., Lintner, B.R., Widlansky, M.J., van der Wiel, K., Dutheil, C., Linsley, B.K., Matthews, A.J., Renwick, J., 2020. South Pacific Convergence Zone dynamics, variability and impacts in a changing climate. Nat. Rev. Earth Environ. 1 (10), 530–543. https://doi.org/10.1038/s43017-020-0078-2.

Camargo, S.J., Sobel, A.H., 2005. Western North Pacific tropical cyclone intensity and ENSO. J. Clim. 18 (15), 2996–3006. https://doi.org/10.1175/JCLI3457.1.

Camargo, S.J., Robertson, A.W., Gaffney, S.J., Smyth, P., Ghil, M., 2007. Cluster analysis of typhoon tracks. Part I: general properties. J. Clim. 20 (14), 3635–3653. https://doi.org/10.1175/JCLI4188.1.

Chan, J.C., 2006. Comment on" Changes in tropical cyclone number, duration, and intensity in a warming environment. Science 311 (5768), 1713. https://doi.org/10.1126/science.1121522, 1713.

Chan, J.C., Williams, R.T., 1987. Analytical and numerical studies of the beta-effect in tropical cyclone motion. Part I: zero mean flow. J. Atmos. Sci. 44 (9), 1257–1265. https://doi.org/10.1175/1520-0469(1987)044<1257:AANSOT>2.0.CO;2.

Chand, S.S., Walsh, K.J., 2009. Tropical cyclone activity in the Fiji region: spatial patterns and relationship to large-scale circulation. J. Clim. 22 (14), 3877–3893. https://doi.org/10.1175/2009JCLI2880.1.

Chand, S.S., Walsh, K.J., 2010. The influence of the Madden–Julian oscillation on tropical cyclone activity in the Fiji region. J. Clim. 23 (4), 868–886. https://doi.org/10.1175/2009JCLI3316.1.

Chand, S.S., Walsh, K.J., 2011. Influence of ENSO on tropical cyclone intensity in the Fiji region. J. Clim. 24 (15), 4096–4108. https://doi.org/10.1175/2011JCLI4178.1.

Chand, S.S., McBride, J.L., Tory, K.J., Wheeler, M.C., Walsh, K.J., 2013. Impact of different ENSO regimes on southwest Pacific tropical cyclones. J. Clim. 26 (2), 600–608. https://doi.org/10.1175/JCLI-D-12-00114.1.

Chand, S.S., Dowdy, A.J., Ramsay, H.A., Walsh, K.J., Tory, K.J., Power, S.B., Bell, S.S., Lavender, S.L., Ye, H., Kuleshov, Y., 2019. Review of tropical cyclones in the Australian region: climatology, variability, predictability, and trends. Wiley Interdiscipl. Rev.: Clim. Change 10 (5), e602. https://doi.org/10.1002/wcc.602.

Chand, S.S., Dowdy, A., Bell, S., Tory, K., 2020. A review of South Pacific tropical cyclones: impacts of natural climate variability and climate change. Clim. Change and Impacts Pac. 251–273. https://doi.org/10.1007/978-3-030-32878-8_6.

Christensen, J.H., Kanikicharla, K.K., Aldrian, E., An, S.I., Cavalcanti, I.F.A., de Castro, M., Dong, W., Goswami, P., Hall, A., Kanyanga, J.K., Kitoh, A., 2013. Climate phenomena and their relevance for future regional climate change. In: Climate Change 2013 the Physical Science Basis: Working Group I Contribution to the Fifth Assessment Report of the Intergovernmental Panel on Climate Change. Cambridge University Press, pp. 1217–1308.

Chu, P.S., 2004. ENSO and Tropical Cyclone Activity. Columbia University Press, New York, pp. 297–332.

Daloz, A.S., Camargo, S.J., 2018. Is the poleward migration of tropical cyclone maximum intensity associated with a poleward migration of tropical cyclone genesis? Clim. Dynam. 50 (1), 705–715. https://doi.org/10.1007/s00382-017-3636-7.

Diamond, H.J., Renwick, J.A., 2015. The climatological relationship between tropical cyclones in the southwest pacific and the Madden–Julian Oscillation. Int. J. Climatol. 35 (5), 676–686. https://doi.org/10.1002/joc.4012.

Diamond, H.J., Lorrey, A.M., Knapp, K.R., Levinson, D.H., 2012. Development of an enhanced tropical cyclone tracks database for the southwest Pacific from 1840 to 2010. Int. J. Climatol. 32, 2240–2250. https://doi.org/10.1002/joc.2412.

Diamond, H.J., Lorrey, A.M., Renwick, J.A., 2013. A southwest Pacific tropical cyclone climatology and linkages to the El Niño–Southern Oscillation. J. Clim. 26 (1), 3–25. https://doi.org/10.1175/JCLI-D-12-00077.1.

Dowdy, A.J., Qi, L., Jones, D., Ramsay, H., Fawcett, R., Kuleshov, Y., 2012. Tropical cyclone climatology of the south Pacific ocean and its relationship to El Niño–Southern Oscillation. J. Clim. 25 (18), 6108–6122. https://doi.org/10.1175/JCLI-D-11-00647.1.

Dvorak, V.F., 1973. A Technique for the Analysis and Forecasting of Tropical Cyclone Intensities from Satellite Pictures. NOAA Tech Memo1972. NESS, pp. 1–20.

Dvorak, V.F., 1975. Tropical cyclone intensity analysis and forecasting from satellite imagery. Mon. Weather Rev. 103 (5), 420–430. https://doi.org/10.1175/1520-0493(1975)103<0420:TCIAAF>2.0.CO;2.

Emanuel, K., 2021. Response of global tropical cyclone activity to increasing CO2: results from downscaling CMIP6 models. J. Clim. 34 (1), 57–70. https://doi.org/10.1175/JCLI-D-20-0367.1.

Folland, C.K., Renwick, J.A., Salinger, M.J., Mullan, A.B., 2002. Relative influences of the interdecadal Pacific oscillation and ENSO on the South Pacific convergence zone. Geophys. Res. Lett. 29 (13) https://doi.org/10.1029/2001GL014201, 21-1.

Gray, W.M., 1975. Tropical Cyclone Genesis, Doctoral Dissertation. Colorado State University. Libraries [Available online at. https://mountainscholar.org/bitstream/handle/10217/247/0234_Bluebook.pdf;sequence=1].

Haffke, C., Magnusdottir, G., 2013. The South Pacific Convergence Zone in three decades of satellite images. J. Geophys. Res. Atmos. 118 (19), 10–839. https://doi.org/10.1002/jgrd.50838.

Hartfield, G., Blunden, J., Arndt, D.S., 2018. State of the climate in 2017. Bull. Am. Meteorol. Soc. 99 (8), Si–S310. https://doi.org/10.1175/2018BAMSStateoftheClimate.1.

Hastings, P.A., 1990. Southern Oscillation influences on tropical cyclone activity in the Australian/south-west Pacific region. Int. J. Climatol. 10 (3), 291–298. https://doi.org/10.1002/joc.3370100306.

Holland, G.J., 1981. On the quality of the Australian tropical cyclone data base. Aust. Met. Mag 29, 169–181.
Iizuka, S., Matsuura, T., 2012. Analysis of Tropical Cyclone Activity in the Southern Hemisphere Using Observation and CGCM Simulation. Cyclones: Formation, Triggers, and Control, 37-35. [available online at: https://www.researchgate.net/publication/307364501_Analysis_of_tropical_cyclone_activity_in_the_Southern_Hemisphere_using_observation_and_CGCM_simulation],.
Jourdain, N.C., Marchesiello, P., Menkès, C.E., Lefèvre, J., Vincent, E.M., Lengaigne, M., Chauvin, F., 2011. Mesoscale simulation of tropical cyclones in the South Pacific: climatology and interannual variability. J. Clim. 24 (1), 3–25. https://doi.org/10.1175/2010JCLI3559.1.
Kimball, S.K., Mulekar, M.S., 2004. A 15-year climatology of North Atlantic tropical cyclones. Part I: size parameters. J. Clim. 17 (18), 3555–3575. https://doi.org/10.1175/1520-0442(2004)017<3555:AYCONA>2.0.CO;2.
Knaff, J.A., Slocum, C.J., Musgrave, K.D., Sampson, C.R., Strahl, B.R., 2016. Using routinely available information to estimate tropical cyclone wind structure. Mon. Weather Rev. 144 (4), 1233–1247. https://doi.org/10.1175/MWR-D-15-0267.1.
Knutson, T., Camargo, S.J., Chan, J.C., Emanuel, K., Ho, C.H., Kossin, J., Mohapatra, M., Satoh, M., Sugi, M., Walsh, K., Wu, L., 2019. Tropical cyclones and climate change assessment: Part I: detection and attribution. Bull. Am. Meteorol. Soc. 100 (10), 1987–2007. https://doi.org/10.1175/BAMS-D-18-0189.1.
Knutson, T., Camargo, S.J., Chan, J.C., Emanuel, K., Ho, C.H., Kossin, J., Mohapatra, M., Satoh, M., Sugi, M., Walsh, K., Wu, L., 2020. Tropical cyclones and climate change assessment: Part II: projected response to anthropogenic warming. Bull. Am. Meteorol. Soc. 101 (3), E303–E322. https://doi.org/10.1175/BAMS-D-18-0194.1.
Kossin, J.P., 2018. A global slowdown of tropical-cyclone translation speed. Nature 558 (7708), 104–107. https://doi.org/10.1038/s41586-018-0158-3.
Kossin, J.P., 2019. Reply to: Moon, I.-J. et al.; Lanzante, JR. Nature 570 (7759), E16–E22. https://doi.org/10.1038/s41586-019-1224-1.
Kossin, J.P., Emanuel, K.A., Vecchi, G.A., 2014. The poleward migration of the location of tropical cyclone maximum intensity. Nature 509 (7500), 349–352. https://doi.org/10.1038/nature13278.
Kostaschuk, R., Terry, J., Raj, R., 2001. Tropical cyclones and floods in Fiji. Hydrol. Sci. J. 46 (3), 435–450. https://doi.org/10.1080/02626660109492837.
Kuleshov, Y., Qi, L., Fawcett, R., Jones, D., 2008. On tropical cyclone activity in the Southern Hemisphere: trends and the ENSO connection. Geophys. Res. Lett. 35 (14) https://doi.org/10.1029/2007GL 032983.
Kuleshov, Y., Chane Ming, F., Qi, L., Chouaibou, I., Hoareau, C., Roux, F., 2009. Tropical cyclone genesis in the Southern Hemisphere and its relationship with the ENSO. June Ann. Geophys. 27 (6), 2523–2538. https://doi.org/10.5194/angeo-27-2523-2009. Copernicus GmbH.
Kuleshov, Y., Fawcett, R., Qi, L., Trewin, B., Jones, D., McBride, J., Ramsay, H., 2010. Trends in tropical cyclones in the south Indian ocean and the south pacific ocean. J. Geophys. Res. Atmos. 115 (D1) https://doi.org/10.1029/2009JD012372.
Kuleshov, Y., Gregory, P., Watkins, A.B., Fawcett, R.J., 2020. Tropical cyclone early warnings for the regions of the Southern Hemisphere: strengthening resilience to tropical cyclones in small island developing states and least developed countries. Nat. Hazards 104 (2), 1295–1313. https://doi.org/10.1007/s11069-020-04214-2.
Lanzante, J.R., 2019. Uncertainties in tropical-cyclone translation speed. Nature 570 (7759), E6–E15. https://doi.org/10.1038/s41586-019-1223-2.
Lavender, S.L., Dowdy, A.J., 2016. Tropical cyclone track direction climatology and its intraseasonal variability in the Australian region. J. Geophys. Res. Atmos. 121 (22), 13–236. https://doi.org/10.1002/2016JD025562.
Magee, A.D., Verdon-Kidd, D.C., 2018. On the relationship between Indian Ocean sea surface temperature variability and tropical cyclogenesis in the southwest Pacific. Int. J. Climatol. 38, e774–e795. https://doi.org/10.1002/joc.5406.
Magee, A.D., Verdon-Kidd, D.C., Kiem, A.S., Royle, S.A., 2016. Tropical cyclone perceptions, impacts and adaptation in the Southwest Pacific: an urban perspective from Fiji, Vanuatu and Tonga. Nat. Hazards Earth Syst. Sci. 16 (5), 1091–1105. https://doi.org/10.5194/nhess-16-1091-2016.
Magee, A.D., Verdon-Kidd, D.C., Diamond, H.J., Kiem, A.S., 2017. Influence of ENSO, ENSO Modoki, and the IPO on tropical cyclogenesis: a spatial analysis of the southwest Pacific region. Int. J. Climatol. 37, 1118–1137. https://doi.org/10.1002/joc.5070.
Magee, A.D., Lorrey, A.M., Kiem, A.S., Colyvas, K., 2020. A new island-scale tropical cyclone outlook for southwest Pacific nations and territories. Sci. Rep. 10 (1), 1–13. https://doi.org/10.1038/s41598-020-67646-7.
Maru, E., Shibata, T., Ito, K., 2018. Statistical analysis of tropical cyclones in the Solomon Islands. Atmosphere 9 (6), 227. https://doi.org/10.3390/atmos9060227.
McInnes, K.L., Walsh, K.J., Hoeke, R.K., O'Grady, J.G., Colberg, F., Hubbert, G.D., 2014. Quantifying storm tide risk in Fiji due to climate variability and change. Global Planet. Change 116, 115–129. https://doi.org/10.1016/j.gloplacha.2014.02.004.
Menkes, C.E., Lengaigne, M., Marchesiello, P., Jourdain, N.C., Vincent, E.M., Lefèvre, J., Chauvin, F., Royer, J.F., 2012. Comparison of tropical cyclogenesis indices on seasonal to interannual timescales. Clim. Dynam. 38 (1–2), 301–321. https://doi.org/10.1007/s00382-011-1126-x.
Moon, I.J., Kim, S.H., Chan, J.C., 2019. Climate change and tropical cyclone trend. Nature 570 (7759), E3–E5. https://doi.org/10.1038/s41586-019-1222-3.
Nerem, R.S., Beckley, B.D., Fasullo, J.T., Hamlington, B.D., Masters, D., Mitchum, G.T., 2018. Climate-change–driven accelerated sea-level rise detected in the altimeter era. Proc. Natl. Acad. Sci. USA 115 (9), 2022–2025. https://doi.org/10.1073/pnas.1717312115.
Nurse, L.A., McLean, R.F., Agard, J., et al., 2014. Small islands. In: Climate Change 2014: Impacts, Adaptation, and Vulnerability. Part B: Regional Aspects. Contribution of Working Group II to the Fifth Assessment Report of the Intergovernmental Panel on Climate Change. Cambridge University Press, Cambridge, UK, pp. 1613–1654 [Available online at: https://www.ipcc.ch/site/assets/uploads/2018/02/WGIIAR5-Chap29_FINAL.pdf.
Pfeffer, J., Spada, G., Mémin, A., Boy, J.P., Allemand, P., 2017. Decoding the origins of vertical land motions observed today at coasts. Geophys. J. Int. 210 (1), 148–165. https://doi.org/10.1093/gji/ggx142.
Ramsay, H., 2017. The global climatology of tropical cyclones. In: Oxford Research Encyclopedia of Natural Hazard Science. https://doi.org/10.1093/acrefore/9780199389407.013.79.
Ramsay, H.A., Doswell III, C.A., 2005. A sensitivity study of hodograph-based methods for estimating supercell motion. Weather Forecast. 20 (6), 954–970. https://doi.org/10.1175/WAF889.1.
Ramsay, H.A., Leslie, L.M., Lamb, P.J., Richman, M.B., Leplastrier, M., 2008. Interannual variability of tropical cyclones in the Australian region: role of large-scale environment. J. Clim. 21 (5), 1083–1103. https://doi.org/10.1175/2007JCLI1970.1.
Ramsay, H.A., Camargo, S.J., Kim, D., 2012. Cluster analysis of tropical cyclone tracks in the Southern Hemisphere. Clim. Dynam. 39 (3–4), 897–917. https://doi.org/10.1007/s00382-011-1225-8.
Salinger, M.J., McGree, S., Beucher, F., Power, S.B., Delage, F., 2014. A new index for variations in the position of the South Pacific convergence zone 1910/11–2011/2012. Clim. Dynam. 43 (3–4), 881–892. https://doi.org/10.1007/s00382-013-2035-y.
Sharma, K.K., Verdon-Kidd, D.C., Magee, A.D., 2020. Decadal variability of tropical cyclogenesis and decay in the southwest Pacific. Int. J. Climatol. 40 (5), 2811–2829. https://doi.org/10.1002/joc.6368.
Sharmila, S., Walsh, K.J.E., 2018. Recent poleward shift of tropical cyclone formation linked to Hadley cell expansion. Nat. Clim. Change 8 (8), 730–736. https://doi.org/10.1038/s41558-018-0227-5.
Sinclair, M.R., 2002. Extratropical transition of southwest Pacific tropical cyclones. Part I: climatology and mean structure changes. Mon. Weather Rev. 130 (3), 590–609. https://doi.org/10.1175/1520-0493(2002)130<0590:ETOSPT>2.0.CO;2.
Singh, A., Delcroix, T., Cravatte, S., 2011. Contrasting the flavors of El Niño-Southern Oscillation using sea surface salinity observations. J. Geophys. Res.: Oceans 116 (C6). https://doi.org/10.1029/2010JC006862.
Tauvale, L., Tsuboki, K., 2019. Characteristics of tropical cyclones in the southwest pacific. J. Meteorol. Soc. Jpn. https://doi.org/10.2151/jmsj.2019-042. *Ser. II.*
Terry, J.P., 2007. Tropical Cyclones: Climatology and Impacts in the South Pacific. Springer Science & Business Media.
Terry, J.P., Gienko, G., 2010. Climatological aspects of South Pacific tropical cyclones, based on analysis of the RSMC-Nadi (Fiji) regional archive. Clim. Res. 42 (3), 223–233. http://www.jstor.org/stable/24870338.
Tonga Government Statistics Department, 2021. Census Preliminary Results November 2021. Available at. https://tongastats.gov.to/census/population-statistics/#22-231-wpfd-2021-1630540712.
Villarini, G., Vecchi, G.A., 2012. North Atlantic power dissipation index (PDI) and accumulated cyclone energy (ACE): statistical modeling and sensitivity to sea surface temperature changes. J. Clim. 25 (2), 625–637. https://doi.org/10.1175/JCLI-D-11-00146.1.
Villarini, G., Smith, J.A., Baeck, M.L., Marchok, T., Vecchi, G.A., 2011. Characterization of rainfall distribution and flooding associated with US landfalling tropical cyclones: analyses of Hurricanes Frances, Ivan, and Jeanne (2004). J. Geophys. Res. Atmos. 116 (D23) https://doi.org/10.1029/2011JD016175.
Vincent, E.M., Lengaigne, M., Menkes, C.E., Jourdain, N.C., Marchesiello, P., Madec, G., 2011. Interannual variability of the South Pacific Convergence Zone and implications for tropical cyclone genesis. Clim. Dynam. 36 (9), 1881–1896. https://doi.org/10.1007/s00382-009-0716-3.
Walsh, K.J., McBride, J.L., Klotzbach, P.J., Balachandran, S., Camargo, S.J., Holland, G., Knutson, T.R., Kossin, J.P., Lee, T.C., Sobel, A., Sugi, M., 2016. Tropical cyclones and climate change. Wiley Interdiscipl. Rev.: Clim. Change 7 (1), 65–89. https://doi.org/10.1016/j.tcrr.2020.01.004.
Wang, C., Wang, X., 2013. Classifying El Niño Modoki I and II by different impacts on rainfall in southern China and typhoon tracks. J. Clim. 26 (4), 1322–1338. https://doi.org/10.1175/JCLI-D-12-00107.1.
Wang, C., Deser, C., Yu, J.Y., DiNezio, P., Clement, A., 2017. El Niño and Southern Oscillation (ENSO): a Review. *Coral reefs of the Eastern Tropical Pacific*, pp. 85–106. https://doi.org/10.1007/978-94-017-7499-4_4.
Wang, B., Luo, X., Yang, Y.M., Sun, W., Cane, M.A., Cai, W., Yeh, S.W., Liu, J., 2019. Historical change of El Niño properties sheds light on future changes of extreme El Niño. Proc. Natl. Acad. Sci. USA 116 (45), 22512–22517. https://doi.org/10.1073/pnas.1911130116.
Weatherford, C.L., Gray, W.M., 1988. Typhoon structure as revealed by aircraft reconnaissance. Part II: structural variability. Mon. Weather Rev. 116 (5), 1044–1056. https://doi.org/10.1175/1520-0493(1988)116<1044:TSARBA>2.0.CO;2.
Webster, P.J., Holland, G.J., Curry, J.A., Chang, H.R., 2005. Changes in tropical cyclone number, duration, and intensity in a warming environment. Science 309 (5742), 1844–1846. https://doi.org/10.1126/science.1116448.
Widlansky, M.J., Annamalai, H., Gingerich, S.B., Storlazzi, C.D., Marra, J.J., Hodges, K.I., Choy, B., Kitoh, A., 2019. Tropical cyclone projections: changing climate threats for Pacific Island defense installations. Weather, clim. soc. 11 (1), 3–15. https://doi.org/10.1175/WCAS-D-17-0112.1.
WMO, 2021. Regional Association V - Tropical Cyclones Operational Pan for the South Pacific and South-East Indian Ocean. *World Meteorological Organization Technical document,* **WMO-No 1181**. https://community.wmo.int/tropical-cyclone-operational-plans.

WMO, 2022. Tropical Cyclones. https://public.wmo.int/en/our-mandate/focus-areas/natural-hazards-and-disaster-risk-reduction/tropicalcyclones#:~:text=Its%20diameter%20is%20 typically%20around,storm%20surges%20and%20coastal%20flooding.
World Bank, 2022. World development indicators. GDP". Available at. https://data.worldbank.org/indicator/NY.GDP.MKTP.CD?locations=TO.
World Trade Organisation (WTO), 2018. Executive summary. Report. Available online at. https://www.wto.org/english/tratop_e/devel_e/study_1_pacific_country_annex_18_april_draft_final.pdf.
Zhang, G., Murakami, H., Knutson, T.R., Mizuta, R., Yoshida, K., 2020. Tropical cyclone motion in a changing climate. Sci. Adv. 6 (17), eaaz7610. https://doi.org/10.1126/sciadv.aaz7610.
Zheng, X.T., 2019. Indo-pacific climate modes in warming climate: consensus and uncertainty across model projections. Curr. Clim. Change Rep. 5 (4), 308–321. https://doi.org/10.1007/s40641-019-00152-9.